International Journal of Scientific & Engineering Research, Volume 5, Issue 5, May-2014
ISSN 2229-5518

A Numerical Investigation on the role of Oil Saturations on Performance of In-Situ Combustion in Porous Media

D. Srinivasa Reddy[a,*], G. Suresh Kumar[b]

[a]Research Scholar, Dept. of Ocean Engg., Indian Institute of Technology Madras, Chennai-600036.
[b]Associate Professor, Dept. of Ocean Engg, Indian Institute of Technology Madras, Chennai-600036.
Email: devarapusrinu@gmail.com[a] , gskumar@iitm.ac.in[b]

* *Corresponding author*

Abstract:

In-Situ Combustion (ISC) is an Enhanced Oil Recovery (EOR) method to increase oil recoveries of heavy oil reservoirs by utilizing heat energy generated by combustion of crude oil inside the porous reservoir. In ISC process a fraction of the Oil Originally In Place (OOIP) is converted into carbon rich residue, also known as coke by thermal cracking and distillation processes. This coke acts as a fuel for sustaining combustion. In flow through porous medium the oil in place are expressed in terms of its saturation (oil saturation), which play an important role in performance of ISC both as primary and/or tertiary recovery method. A numerical model based on block centered finite difference methods is developed to analyze the effect of the initial oil saturation on ISC performance. The numerical results indicate the role of initial oil saturation on critical parameters of ISC: fuel depositions, average peak temperatures, combustion front propagation and oil production rates. Especially at high oil saturations an oil bank forms ahead of combustion front with almost negligible gas permeability causing significant fluctuations in reservoir pressure. This oil blockage further decreases the mobility of oil and combustion front velocity, causing a drastic increase in the production timings. The combustion front velocity is reduced from 0.28 m/day at 30% to 0.18m/day at 60% initial oil saturation. The average peak temperatures are found to increase by 36 K, when the oil saturation is increased from 50% to 60%.

Key Words: Numerical Modeling, Porous Media, Combustion/Oxidation, Oil Saturation and Thermal Front

Introduction

Global energy consumptions are estimated to increase from 524 quadrillion Btu in 2010 to 630 quadrillion Btu in 2020 (DOE/EIA (2013)). Oil and gas takes major share in fulfilling world energy demands. An analysis of global oil resources to meet this energy demands estimated an ultimate recoverable oil reserves of 1.68 trillion tons. Assuming that the estimated recoverable oil reserves are presently one third of the original oil in-place, the oil in place, regardless of recoverability, is assessed at 5 trillion tons or 37 trillion bbls. Now, every 1% increase in oil recovery will add 5 trillion tons to the total oil production. Any technique that could increase the total recovery factor by 10% would bring an increase of 50 billion tons of oil, which corresponds to a 50% increase in the present amount of recoverable oil reserve. Enhanced oil recovery methods aim to recover this remaining oil in place and have the potential to reclassify the unrecoverable and contingent reserves (Green and Wilhite (1999)). The quantities of oil in reservoirs expressed as oil saturations (especially residual oil saturation) decides the performance of EOR method applied.

EOR methods focus on improving the oil recoveries by increasing either displacement efficiency by reducing residual oil saturation in swept regions or sweep efficiency by displacing the remaining oil in unswept regions. Residual oil saturation is a function of capillary number, which is the ratio of viscous force to capillary force. Typically, the capillary number for water flooding is confined to below 10^{-6}, usually to 10^{-7}. The capillary number increases in effective EOR application by three orders of magnitudes to about 10^{-3} to 10^{-4}. The capillary number can be significantly reduced by either lowering the interfacial tension or altering the rock wettability to a more water-wet surface or by increasing the viscous forces(Green and Wilhite (1999)). Oil in unswept regions can be recovered by any or all mechanisms such as: increasing the viscosity of the displacing fluid; reducing oil viscosity; modifying permeability and altering wettability.

Thermal Enhanced oil recovery methods improve oil recoveries primarily by decreasing oil viscosities and account for more than 60% of all EOR oil production in the USA (Farouq Ali and Thomas (1994)). Thermal methods involving steam/hot water injection or in-situ

combustion are primarily intended for heavy oils (10^0 – 20^0 API) and are characterized by the input of energy into the reservoir, either by injecting hot fluid or through in-situ chemical reaction between crude oil and oxygen.

The steam drive process is much like a conventional water-flood, in which steam is injected into several injection wells while oil is produced from other wells. Thermal energy contributed by steam is used to heat the reservoir oil. Steam applications have been limited to shallow reservoirs because as the steam is injected in deep reservoirs, it loses heat energy in the well bore, and all the steam will be converted into liquid water. Steam drives have been applied in many pilot and field scale projects with very good success.

In-situ combustion is a displacement process in which an oxygen containing gas is injected into a reservoir where it reacts with the crude oil to create a high temperature combustion front that is propagated through the reservoir. Ignition may be induced through electrical or gas igniters or may be spontaneous if the crude oil has sufficient reactivity (Ramey et al (1992)). High temperature during burning causes the lighter fractions of oil ahead of the flame to vaporize, leaving a heavy residual coke or carbon- deposit as fuel to be burned. This residuum becomes the fuel for the process. In-situ combustion is possible if the crude oil/rock combination produces enough fuel to sustain the combustion front (Graves et al (2000)). In general, no more than 5% to 6% of the oil is consumed. Hydrocarbon products and other compounds released by the cracking process (SO_2, CO, CH_4, and H_2) join the combustion gases and are either absorbed by crude oil ahead of the front or are produced in the effluent. The hot produced gases (vaporized light components) and steam formed by combustion and vaporization of connate water, move forward displacing the oil with it. Upon contacting the cooler portions of the reservoir, the gases and vapors condense. The combustion front moves forward through the reservoir only after burning all deposited fuel. This fuel represents the least desirable portion of the crude under ideal conditions.

Ramey et al (1992) compared the thermal efficiency of steam and in-situ combustion in an analysis of the energy requirements for thermal oil recovery in the South Belridge field. On the basis of observations on field performance, in-situ combustion required about 4 Mscf air/bbl oil, which corresponds to a fuel requirement of about 288,000 Btu fuel/bbl oil. Steam stimulation has resulted in a steam/oil ratio of 0.35 or an energy requirement of 1,400,000 Btu fuel/ bbl oil. Thus, approximately 4.9 times as much energy per barrel oil is required for steam injection as for in-situ combustion. On the other hand, steam flooding has been successful in a number of light oil reservoirs; in-situ combustion seems to work best for deep, high-pressure reservoirs with moderately heavy oils, with high thermal efficiency among all the known thermal recovery methods (Butler (1997)).

Although thermal efficiency favours in-situ combustion, field scale in-situ combustion projects represent about 3% of the oil produced by thermal-recovery processes. This is because of the difficulty in understanding the complex phenomena that occur during in-situ combustion and lack of reliable methods for predicting the performance. Numerical modelling is a powerful tool in identifying the key factors affecting the performance of the complex thermal process occurring in porous media and is helpful in making intelligent decisions regarding the process operations. The Present work will focus on the numerical modelling of non-isothermal multi-phase systems emerging during in-situ combustion thermal recovery processes into porous media and aims at evaluating the performance of ISC under varying initial oil saturations.

The Physical and Numerical Model

The physical model considers multi phase flow of heavy oil, water (aqueous phase), vapor and coke in porous reservoirs. A part of the oil is allowed to undergo oxidation and/or combustion by injecting oxygen (or air) into the reservoir. The heat released from the exothermic combustion reaction is utilized in reducing the viscosity of the heavy oil, promoting easy flow of heavy oil to the production well. The oil is assumed to undergo cracking/pyrolysis producing light cracked components and a solid component known as coke. The kinetic model representing the sequence of reactions is same as that developed by Crookston et al (1979).

Oil is assumed to be immiscible with water (aqueous) phase. The oil phase is lumped into 2 components: heavy oil and light oil components. The physical properties of dodecane and propane are used for heavy oil and light oil, respectively. All the gaseous components produced during the thermal process are lumped into inert gas. The oil components and water are assumed to be in liquid and vapor phases. The distillation effects of oil components along with vaporization and condensation of water are governed by vapor-liquid equilibria. The coke is assumed to be immobile and responsible for sustaining the combustion (Fassihi et al (1984), Greaves et al (2000)). The characteristics of reservoir along with reservoir fluids are reported in Table 1.

Table 1

The physical system considers advective-diffusive-reactive flow of heat and mass through porous medium. The system is assumed to be under thermal equilibrium and the heat transport is assumed to take place by conduction and convection. The capillary effects among the oil-water-gas phases are calculated using Coats (1980) method. The coupled partial differential equations that describe the conservation of component mass and energy are similar to those used by Crookston et al. (1979), and Rubin and Vinsome (1980). All physical properties and chemical reaction rates are allowed to be functions of the dependent variables and are taken from Crookston et al (1979), Grabowski et al (1979) and Coats (1980).

The numerical scheme is based on block-centered, finite-difference methods. The equations are discretized using standard central difference approximations in space and two-point backward differences in time. The coupled nonlinear algebraic equations resulting from finite difference discretization are listed in Appendix and are solved by Newton-Raphson iterative scheme (Rubin and Buchannan (1985)) for the primary dependent variables.

Results and Discussion:

Figure 1

Figure 1 shows the comparison between the cumulative heavy oil recovery obtained from the present numerical model and the recovery reported by Crookston et al (1979). The recovery of heavy oil component is calculated as percent of original oil in place (OOIP). Oil saturation for the base case is maintained at 50%. Initial oil in place is $2.5272*10^3$ stock tank m^3 of heavy oil with no light oil originally present (as seen in table 1). The numerical results show that, about 83.4% of OOIP is recovered as heavy oil. The numerical results exhibited good agreement with those reported by Crookston et al (1979). A cumulative oil recovery of about 98.7% of OOIP was recorded in about 157 days against 97% oil recovery reported by Crookston et al (1979) in about 150 days.

Figure 2

Figure 2 shows the effect of variation in initial oil saturation on oil saturation distribution during the ISC process. Oil saturation is expressed as the fraction of oil present in the reservoir pores and is plotted at a location 22.5 m from injection well. The numerical results show prolonged oil saturation profiles with increased initial oil saturations, which are an indicative of decreased mobility of oil phase, resulting in delayed production rates at the production well. Especially at high oil saturations, the numerical results indicate negligible gas permeability due to the blockage caused by a thick oil bank formed from condensation of oil mobilized ahead of combustion front. An increase in production periods at the production well confirms the decrease in this mobility (as seen in figures 6, 7 and 8).

Figure 3

Figure 4

Figure 3 represents the temporal distribution of coke concentration at various initial oil saturations. The coke concentration is expressed as amount of coke present in gram moles per unit volume of formation and is plotted at a distance of 22.5 m from injection well. The concentrations result from deposition of coke by cracking reaction and its consumption by oxidation reaction. The numerical results show an increase in coke concentration with an increase in the initial oil saturation. The fact that an increase in the initial oil saturation allows for additional oil availability for cracking reaction results in added amounts of coke deposits. The oxygen availability for coke oxidation reaction decreased in comparison with the oxygen availability for the same reaction at lower oil saturations, owing to the fact that the oxygen flow rate at the injection well is maintained constant for all the cases. Further, an increase in oxygen consumption with an increase in heavy oil quantities in its oxidation along with light oil results in a more or less, lower coke consumption rates. The increase in coke deposits acting as a fuel for combustion results in elevated peak temperatures as seen in figure 4, showing the effect of initial oil saturation on temporal distribution of thermal fronts. The temperature profiles are also plotted at the same location of coke concentration distribution. It is evident from figure 4 that the peak temperatures occurring in the combustion zone increase with increased coke depositions caused due to increase in initial oil saturations.

It is further observed that the thermal fronts recorded high average peak temperatures at delayed combustion front velocities across the reservoir. The combustion front velocity is calculated using coats (1980) method and is expressed as ratio of 0.5*length of the reservoir and the difference between the time taken to record peak temperatures at 2^{nd} block and the $n\text{-}1^{th}$ block. Numerical results show an increase in the average peak temperature of about 36 K (660.4 K to 696.3 K) when the initial oil saturation is increased from 50% to 60%. Similarly the combustion velocity slows down from 0.025m/day (0.213 m/day at 50% to 0.188 m/day at 60% initial oil saturation).

Figure 5

Figure 5 shows the effect of initial oil saturation on the temporal distribution reservoir pressure. The reservoir

pressures profiles are plotted at the same location of coke concentration and temperature profiles (22.5 m from injection well). The numerical results report significant fluctuations in reservoir pressures with increasing oil saturations. These fluctuations are mainly due to the blockage of oil, additional coke depositions and the temperature rise associated with the increased oil quantities. An abrupt drop in reservoir pressure from 6650 kPa on about 27th day to 3360 kPa on about 40th day is observed when the initial oil saturation is maintained at 60%. It can be observed from figure 5 that the reservoir pressure dropped abruptly from 6650 kPa on about 27th day to 3360 kPa on about 40th day, which corresponds to a period when the oil saturations rise to the maximum (as seen in figure 2) and coke oxidation reaction consumes maximum coke (from 2.27 milli-gmol/m^3.day to 2.64 gmol/m^3.day). Further the variations in phase permeabilities cause such fluctuations in reservoir pressure.

Figure 6

Figure 6 shows the effect of initial oil saturation on volumetric production of total oil in liquid phase. As the initial oil in place is completely heavy oil, an increase in the initial oil saturation amounts for an increase in the heavy oil component with higher viscosity. Availability of higher amounts of oil eventually results in higher total oil production, but at the cost of time. The total oil production is calculated as cumulative volumes expressed in cubic meter is the sum of volumes of two pseudo components (heavy oil and light oil components) producing at the production well. An increase in oil saturations with coke concentrations reduces the effective permeability, which delays the oil production rates. Total oil volume of 1900 m^3 is produced in 157 days when the initial oil saturation was 50% (base case), whereas it took about 184 days to produce 2794 m^3 of total oil when the initial oil saturation was raised by 10% (50% to 60%).

Figure 7

Figure 8

Availability of larger volumes of original oil in place in the form of heavy oil also contributes to an increase in cumulative oil recovery of heavy oil components as shown in figure 7 representing the heavy oil components production at the production well. The numerical results show an increase in cumulative recovery of heavy oil component along with a more or less delayed production of light oil component with increase in oil saturation as shown in figure 8, representing the light oil components production at the production well. As the mole fraction of initial light oil component is zero, it production is entirely attributed by cracking of heavy oil component. The delay in light oil component production corresponds to this fact that its entire production is from delayed cracking reaction. The numerical results further show a slight decrease in cumulative recovery of light oil component even at increased oil saturation, because most of the heavy oil is consumed in coke deposition.

Conclusions:

The numerical model developed investigates the effect of initial oil saturations on different aspects of in-situ combustion process. To gain confidence on the model, it is first validated with heavy oil recoveries reported for dry forward combustion simulation. Four initial oil saturation values ranging from 30% to 60% with an increment of 10% are selected. From the sensitivity studies, it can be concluded that the initial oil saturation, which is a measure of oil originally in place significantly affects the major parameters like coke concentrations, reservoir pressures, thermal fronts and oil production rates.

- The numerical results report an increase in cumulative heavy oil recoveries expressed as percent of OOIP by about 10-15% for 10% increase in initial oil saturations.
- The total oil production volumes are observed to increase by about 47% with a delayed time period of about a month when the initial oil saturation is raised from 50% to 60%.
- The numerical results show negligible gas permeability due to the blockage of thick oil bank forming form condensation of oil mobilized ahead of combustion front, causing significant fluctuations in reservoir pressure.
- An average reduction in combustion front velocity of about 0.03 m/day is observed for 10% increase in initial oil saturation.
- A drastic change in average peak temperature of about 50 K is observed when the oil saturation is increased from 30% to 60%.

From our present numerical study, we suggest a further investigation of the effect of additional drive mechanism attributed by water saturation on reservoir pressures, thermal fronts and oil recovery rates.

References:

1. Butler, R. M., 1997. Thermal Recovery of Oil and Bitumen. Grav Drain's Black Book.
2. Central Intelligence Agency. "CIA World Factbook: USA." CIA: The World Factbook, 2011. CIA – The World Factbook.
3. Coats, K.H., 1980. In-situ combustion model. Soc. Pet. Eng. J. 20 (6), 533-554.

4. Crookston, R.B., Culham, W.E., Chen. W.H., 1979. Numerical simulation model for thermal recovery process. Soc. Pet. Eng. J. 19 (1), 37-58.
5. Farouq Ali, S.M., and Thomas, S., 1994. A Realistic Look at Enhanced Oil Recovery. Sciatica Ironical. 1, 219-230.
6. Fasshihi, M.R., Brigham,W.E., and Ramey, Jr.,H.J., 1984. Reaction kinetics of in-situ combustion: Part 1-observations. Paper SPE–9454, presented at the 55th annual fall technical conference and exhibition of the society of petroleum engineers of AMIE, Dallas, Texas.
7. Grabowski, J.W., Vinsome, P.K., Behie, A., Rubin, B., 1979. A fully implicit general purpose finite difference thermal model for in-situ combustion and steam. Paper SPE-8396 presented at the 54th Annual Fall Meeting of SPE, Las Vegas.
8. Green, D.W., and wilhite, G.P., 1999. Enhanced oil Recovery. SPE Dallas, Texas.
9. Greaves, M., Young, T.J., El-Usta, S. Rathbone, R.R., Ren. S.R., and Xia, T.S., 2000. Air injection into light and medium heavy oil reservoirs: combustion tube studies on west of Shetlands Clair oil and light Australian oil. Chem. Engg. Res. Des., 78(A), 721-730.
10. International Energy Outlook 2010, Energy Information Administration, U.S. Department of Energy, June 2010. EIA– oil and coal.
11. International Energy Outlook 2013, Energy Information Administration, U.S. Department of Energy, July 2013. DOE/EIA 0484(2013).
12. Prats, M., 1986. Thermal recovery. Soc. of Pet. Engg. SPE Monograph series. Vol.7
13. Ramey, Jr.,H.J., Stamp, V.W., Pebdani F.N., 1992. Case History of South Belridge, California, InSitu Combustion Oil Recovery. Paper SPE-24200 presented at the SPE/DOE Enhanced Oil Recovery Symposium, Tulsa, April 22-24.
14. Rubin, B., Buchannan, W.L., 1985. A general purpose thermal model. Soc. Pet. Eng. J. 25 (2), 202-214.
15. Rubin, B., Vinsome, P.K.W., 1980. The simulation of the in-situ combustion process in one dimension using a highly implicit finite difference scheme. J. Can. Pet. Tech. 19 (4), 68-76.
16. Sarathi, P.S., 1999. In-situ combustion handbook-principles and practices. Technical Report, U.S. Department of Energy. DOE/PC/91008-0374.

Appendix

The Discretized equations are as follows:

Oil components mass balance:

$$\frac{\mathbf{V}}{\Delta \mathbf{t}}\left[\left(\boldsymbol{\varphi}^{\mathbf{n+1}}\boldsymbol{\rho}_{\mathbf{o_i}}^{\mathbf{n+1}}\mathbf{s}_{\mathbf{o_i}}^{\mathbf{n+1}}\mathbf{X}_{\mathbf{o_i}}^{\mathbf{n+1}}-\boldsymbol{\varphi}^{\mathbf{n}}\boldsymbol{\rho}_{\mathbf{o_i}}^{\mathbf{n}}\mathbf{s}_{\mathbf{o_i}}^{\mathbf{n}}\mathbf{X}_{\mathbf{o_i}}^{\mathbf{n}}\right)+\left(\boldsymbol{\varphi}^{\mathbf{n+1}}\boldsymbol{\rho}_{\mathbf{g_i}}^{\mathbf{n+1}}\mathbf{s}_{\mathbf{g_i}}^{\mathbf{n+1}}\mathbf{Y}_{\mathbf{g_i}}^{\mathbf{n+1}}-\boldsymbol{\varphi}^{\mathbf{n}}\boldsymbol{\rho}_{\mathbf{g_i}}^{\mathbf{n}}\mathbf{s}_{\mathbf{g_i}}^{\mathbf{n}}\mathbf{Y}_{\mathbf{g_i}}^{\mathbf{n}}\right)\right]=\boldsymbol{\tau}_{\mathbf{o_i}}^{\mathbf{n+1}}\mathbf{X}_{\mathbf{o_i}}^{\mathbf{n+1}}\left(\boldsymbol{\Phi}_{\mathbf{o_{i+1}}}^{\mathbf{n+1}}-\boldsymbol{\Phi}_{\mathbf{o_i}}^{\mathbf{n+1}}\right)$$
$$+\boldsymbol{\tau}_{\mathbf{o_{i-1}}}^{\mathbf{n+1}}\mathbf{X}_{\mathbf{o_{i-1}}}^{\mathbf{n+1}}\left(\boldsymbol{\Phi}_{\mathbf{o_{i-1}}}^{\mathbf{n+1}}-\boldsymbol{\Phi}_{\mathbf{o_i}}^{\mathbf{n+1}}\right)+\boldsymbol{\tau}_{\mathbf{g_i}}^{\mathbf{n+1}}\mathbf{Y}_{\mathbf{o_i}}^{\mathbf{n+1}}\left(\boldsymbol{\Phi}_{\mathbf{g_{i+1}}}^{\mathbf{n+1}}-\boldsymbol{\Phi}_{\mathbf{g_i}}^{\mathbf{n+1}}\right)+\boldsymbol{\tau}_{\mathbf{g_{i-1}}}^{\mathbf{n+1}}\mathbf{Y}_{\mathbf{o_{i-1}}}^{\mathbf{n+1}}\left(\boldsymbol{\Phi}_{\mathbf{g_{i-1}}}^{\mathbf{n+1}}-\boldsymbol{\Phi}_{\mathbf{g_i}}^{\mathbf{n+1}}\right)+\mathbf{Q}_{\mathbf{o_i}}^{\mathbf{n+1}}+\sum\mathbf{s}\,\mathbf{r}_{\mathbf{k_i}}^{\mathbf{n+1}}$$

Water components mass balance:

$$\frac{\mathbf{V}}{\Delta \mathbf{t}}\left[\left(\boldsymbol{\varphi}^{\mathbf{n+1}}\boldsymbol{\rho}_{\mathbf{w_i}}^{\mathbf{n+1}}\mathbf{s}_{\mathbf{w_i}}^{\mathbf{n+1}}-\boldsymbol{\varphi}^{\mathbf{n}}\boldsymbol{\rho}_{\mathbf{w_i}}^{\mathbf{n}}\mathbf{s}_{\mathbf{w_i}}^{\mathbf{n}}\right)+\left(\boldsymbol{\varphi}^{\mathbf{n+1}}\boldsymbol{\rho}_{\mathbf{g_i}}^{\mathbf{n+1}}\mathbf{s}_{\mathbf{g_i}}^{\mathbf{n+1}}\mathbf{Y}_{\mathbf{w_i}}^{\mathbf{n+1}}-\boldsymbol{\varphi}^{\mathbf{n}}\boldsymbol{\rho}_{\mathbf{g_i}}^{\mathbf{n}}\mathbf{s}_{\mathbf{g_i}}^{\mathbf{n}}\mathbf{Y}_{\mathbf{w_i}}^{\mathbf{n}}\right)\right]=\boldsymbol{\tau}_{\mathbf{w_i}}^{\mathbf{n+1}}\left(\boldsymbol{\Phi}_{\mathbf{w_{i+1}}}^{\mathbf{n+1}}-\boldsymbol{\Phi}_{\mathbf{w_i}}^{\mathbf{n+1}}\right)+\boldsymbol{\tau}\mathbf{T}_{\mathbf{w_{i-1}}}^{\mathbf{n+1}}\left(\boldsymbol{\Phi}_{\mathbf{w_{i-1}}}^{\mathbf{n+1}}-\boldsymbol{\Phi}_{\mathbf{w_i}}^{\mathbf{n+1}}\right)$$
$$+\boldsymbol{\tau}_{\mathbf{g_i}}^{\mathbf{n+1}}\mathbf{Y}_{\mathbf{w_i}}^{\mathbf{n+1}}\left(\boldsymbol{\Phi}_{\mathbf{g_{i+1}}}^{\mathbf{n+1}}-\boldsymbol{\Phi}_{\mathbf{g_i}}^{\mathbf{n+1}}\right)+\boldsymbol{\tau}_{\mathbf{g_{i-1}}}^{\mathbf{n+1}}\mathbf{Y}_{\mathbf{w_{i-1}}}^{\mathbf{n+1}}\left(\boldsymbol{\Phi}_{\mathbf{g_{i-1}}}^{\mathbf{n+1}}-\boldsymbol{\Phi}_{\mathbf{g_i}}^{\mathbf{n+1}}\right)+\mathbf{Q}_{\mathbf{w_i}}^{\mathbf{n+1}}+\sum\mathbf{s}\,\mathbf{r}_{\mathbf{k_i}}^{\mathbf{n+1}}$$

Non-condensable gas components mass balance:

$$\frac{\mathbf{V}}{\Delta \mathbf{t}}\left(\boldsymbol{\varphi}^{\mathbf{n+1}}\boldsymbol{\rho}_{\mathbf{g_i}}^{\mathbf{n+1}}\mathbf{s}_{\mathbf{g_i}}^{\mathbf{n+1}}\mathbf{Y}_{\mathbf{g_i}}^{\mathbf{n+1}}-\boldsymbol{\varphi}^{\mathbf{n}}\boldsymbol{\rho}_{\mathbf{g_i}}^{\mathbf{n}}\mathbf{s}_{\mathbf{g_i}}^{\mathbf{n}}\mathbf{Y}_{\mathbf{g_i}}^{\mathbf{n}}\right)=\boldsymbol{\tau}_{\mathbf{g_i}}^{\mathbf{n+1}}\mathbf{Y}_{\mathbf{g_i}}^{\mathbf{n+1}}\left(\boldsymbol{\Phi}_{\mathbf{g_{i+1}}}^{\mathbf{n+1}}-\boldsymbol{\Phi}_{\mathbf{g_i}}^{\mathbf{n+1}}\right)+\boldsymbol{\tau}_{\mathbf{g_{i-1}}}^{\mathbf{n+1}}\mathbf{Y}_{\mathbf{g_{i-1}}}^{\mathbf{n+1}}\left(\boldsymbol{\Phi}_{\mathbf{g_{i-1}}}^{\mathbf{n+1}}-\boldsymbol{\Phi}_{\mathbf{g_i}}^{\mathbf{n+1}}\right)+\mathbf{Q}_{\mathbf{g_i}}^{\mathbf{n+1}}+\sum\mathbf{s}\,\mathbf{r}_{\mathbf{k_i}}^{\mathbf{n+1}}$$

Solid phase component (Coke) mass balance

$$\frac{\mathbf{V}}{\Delta \mathbf{t}}\left(\mathbf{C}_{\mathbf{c_i}}^{\mathbf{n+1}}-\mathbf{C}_{\mathbf{c_i}}^{\mathbf{n}}\right)=\sum\mathbf{s}\,\mathbf{r}_{\mathbf{k_i}}^{\mathbf{n+1}}$$

Energy balance:

$$\frac{\mathbf{V}}{\Delta \mathbf{t}}\left((\mathbf{1}-\boldsymbol{\varphi}^{\mathbf{n+1}})\boldsymbol{\rho}_{\mathbf{r_i}}^{\mathbf{n+1}}\mathbf{U}_{\mathbf{r_i}}^{\mathbf{n+1}}-(\mathbf{1}-\boldsymbol{\varphi}^{\mathbf{n}})\boldsymbol{\rho}_{\mathbf{r_i}}^{\mathbf{n}}\mathbf{U}_{\mathbf{r_i}}^{\mathbf{n}}\right)+\left(\boldsymbol{\varphi}^{\mathbf{n+1}}\boldsymbol{\rho}_{\mathbf{o_i}}^{\mathbf{n+1}}\mathbf{s}_{\mathbf{o_i}}^{\mathbf{n+1}}\mathbf{X}_{\mathbf{o_i}}^{\mathbf{n+1}}-\boldsymbol{\varphi}^{\mathbf{n}}\boldsymbol{\rho}_{\mathbf{o_i}}^{\mathbf{n}}\mathbf{s}_{\mathbf{o_i}}^{\mathbf{n}}\mathbf{X}_{\mathbf{o_i}}^{\mathbf{n}}\right)+\left(\boldsymbol{\varphi}^{\mathbf{n+1}}\boldsymbol{\rho}_{\mathbf{g_i}}^{\mathbf{n+1}}\mathbf{s}_{\mathbf{g_i}}^{\mathbf{n+1}}\mathbf{Y}_{\mathbf{g_i}}^{\mathbf{n+1}}-\boldsymbol{\varphi}^{\mathbf{n}}\boldsymbol{\rho}_{\mathbf{g_i}}^{\mathbf{n}}\mathbf{s}_{\mathbf{g_i}}^{\mathbf{n}}\mathbf{Y}_{\mathbf{g_i}}^{\mathbf{n}}\right)$$
$$+\left(\boldsymbol{\varphi}^{\mathbf{n+1}}\boldsymbol{\rho}_{\mathbf{g_i}}^{\mathbf{n+1}}\mathbf{s}_{\mathbf{g_i}}^{\mathbf{n+1}}\mathbf{Y}_{\mathbf{w_i}}^{\mathbf{n+1}}-\boldsymbol{\varphi}^{\mathbf{n}}\boldsymbol{\rho}_{\mathbf{g_i}}^{\mathbf{n}}\mathbf{s}_{\mathbf{g_i}}^{\mathbf{n}}\mathbf{Y}_{\mathbf{w_i}}^{\mathbf{n}}\right)+\left(\boldsymbol{\varphi}^{\mathbf{n+1}}\boldsymbol{\rho}_{\mathbf{c_i}}^{\mathbf{n+1}}\mathbf{U}_{\mathbf{c_i}}^{\mathbf{n+1}}-\boldsymbol{\varphi}^{\mathbf{n}}\boldsymbol{\rho}_{\mathbf{c_i}}^{\mathbf{n}}\mathbf{U}_{\mathbf{c_i}}^{\mathbf{n}}\right)]$$
$$=\mathbf{K}_{\mathbf{f_i}}^{\mathbf{n+1}}\left(\mathbf{T}_{\mathbf{i+1}}^{\mathbf{n+1}}-\mathbf{T}_{\mathbf{i}}^{\mathbf{n+1}}\right)+\mathbf{K}_{\mathbf{f_{i-1}}}^{\mathbf{n+1}}\left(\mathbf{T}_{\mathbf{i-1}}^{\mathbf{n+1}}-\mathbf{T}_{\mathbf{i}}^{\mathbf{n+1}}\right)+\boldsymbol{\tau}_{\mathbf{o_i}}^{\mathbf{n+1}}\mathbf{h}_{\mathbf{o_i}}^{\mathbf{n+1}}\left(\boldsymbol{\Phi}_{\mathbf{o_{i+1}}}^{\mathbf{n+1}}-\boldsymbol{\Phi}_{\mathbf{o_i}}^{\mathbf{n+1}}\right)+\boldsymbol{\tau}_{\mathbf{o_{i-1}}}^{\mathbf{n+1}}\mathbf{h}_{\mathbf{o_{i-1}}}^{\mathbf{n+1}}\left(\boldsymbol{\Phi}_{\mathbf{o_{i-1}}}^{\mathbf{n+1}}-\boldsymbol{\Phi}_{\mathbf{o_i}}^{\mathbf{n+1}}\right)$$
$$+\boldsymbol{\tau}_{\mathbf{g_i}}^{\mathbf{n+1}}\mathbf{h}_{\mathbf{g_i}}^{\mathbf{n+1}}\left(\boldsymbol{\Phi}_{\mathbf{g_{i+1}}}^{\mathbf{n+1}}-\boldsymbol{\Phi}_{\mathbf{g_i}}^{\mathbf{n+1}}\right)+\boldsymbol{\tau}_{\mathbf{g_{i-1}}}^{\mathbf{n+1}}\mathbf{h}_{\mathbf{g_{i-1}}}^{\mathbf{n+1}}\left(\boldsymbol{\Phi}_{\mathbf{g_{i-1}}}^{\mathbf{n+1}}-\boldsymbol{\Phi}_{\mathbf{g_i}}^{\mathbf{n+1}}\right)+\boldsymbol{\tau}_{\mathbf{w_i}}^{\mathbf{n+1}}\mathbf{h}_{\mathbf{w}}^{\mathbf{n+1}}\left(\boldsymbol{\Phi}_{\mathbf{w_{i+1}}}^{\mathbf{n+1}}-\boldsymbol{\Phi}_{\mathbf{w_i}}^{\mathbf{n+1}}\right)$$
$$+\boldsymbol{\tau}_{\mathbf{w_{i-1}}}^{\mathbf{n+1}}\mathbf{h}_{\mathbf{w_{i-1}}}^{\mathbf{n+1}}\left(\boldsymbol{\Phi}_{\mathbf{w_{i-1}}}^{\mathbf{n+1}}-\boldsymbol{\Phi}_{\mathbf{w_i}}^{\mathbf{n+1}}\right)+(\mathbf{Q}_{\mathbf{o_i}}^{\mathbf{n+1}}\dot{\mathbf{h}}_{\mathbf{o_i}}^{\mathbf{n+1}}+\mathbf{Q}_{\mathbf{g_i}}^{\mathbf{n+1}}\dot{\mathbf{h}}_{\mathbf{g_i}}^{\mathbf{n+1}}+\mathbf{Q}_{\mathbf{w_i}}^{\mathbf{n+1}}\dot{\mathbf{h}}_{\mathbf{w_i}}^{\mathbf{n+1}})+\sum\mathbf{H}_{\mathbf{i}}^{\mathbf{n+1}}\,\mathbf{r}_{\mathbf{k}}^{\mathbf{n+1}}$$

Where k denote reaction, i and n denote pace and time, v velocity, τ transmissibility, Φ the head, V block volume, Q volumetric rate, ϕ porosity, ϱ density, S saturation, r reaction rate, U internal energy, h enthalpy, H heat of reaction.

Tables:

Table 1. Characteristics of reservoir and reservoir fluids.

S.No.	Reservoir and Reservoir Fluid Property	Value
1	Porosity	0.38
2	Permeability, m^2	4E-12
3	Initial temperature, K	367
4	Initial Pressure, kPa	455
5	Well back flow pressure, kPa	410
6	Oxygen Injection rate, g.mol/day	1.36E5
7	Injection temperature, K	367
8	Initial mole fraction of Heavy oil	1.0
9	Initial mole fraction of light oil	0.0
10	Initial coke saturation	0.0
11	Initial water saturation	0.2
12	Initial gas saturation	0..3

Figures:

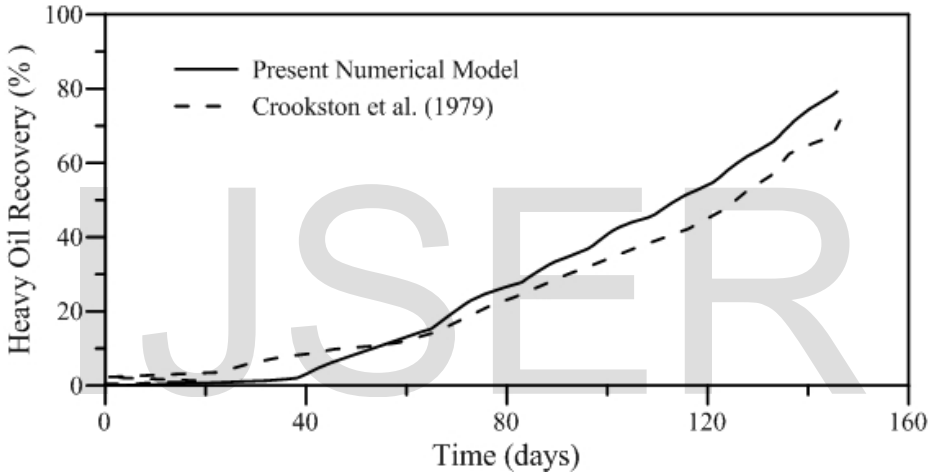

Figure 1. Comparison of heavy oil component production from present numerical model with Crookston et al (1979).

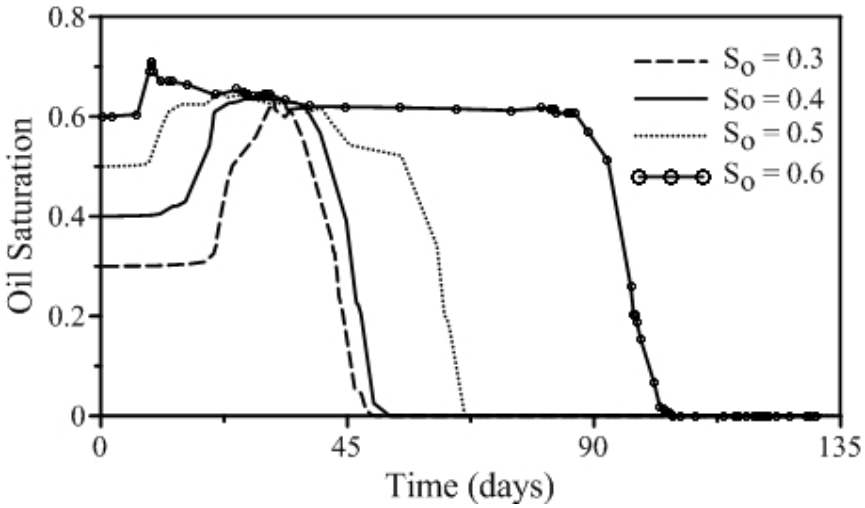

Figure 2. Effect of initial oil saturation on temporal distribution of oil saturation resulting during ISC process.

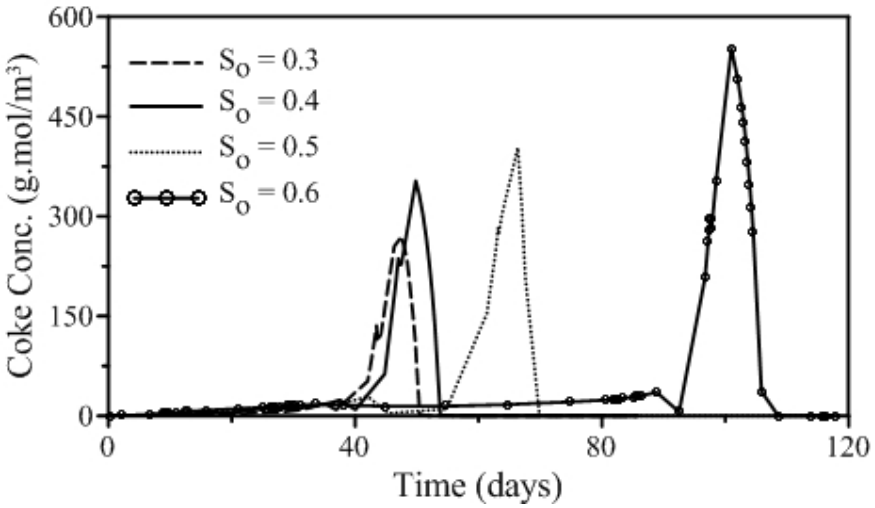

Figure 3. Effect of initial oil saturation on temporal distribution coke concentrations.

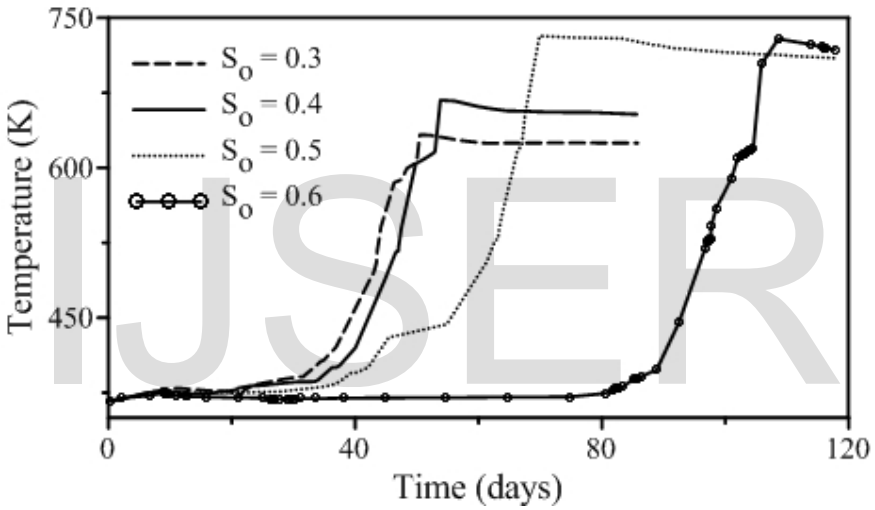

Figure 4. Effect of initial oil saturation on temporal distribution of temperature.

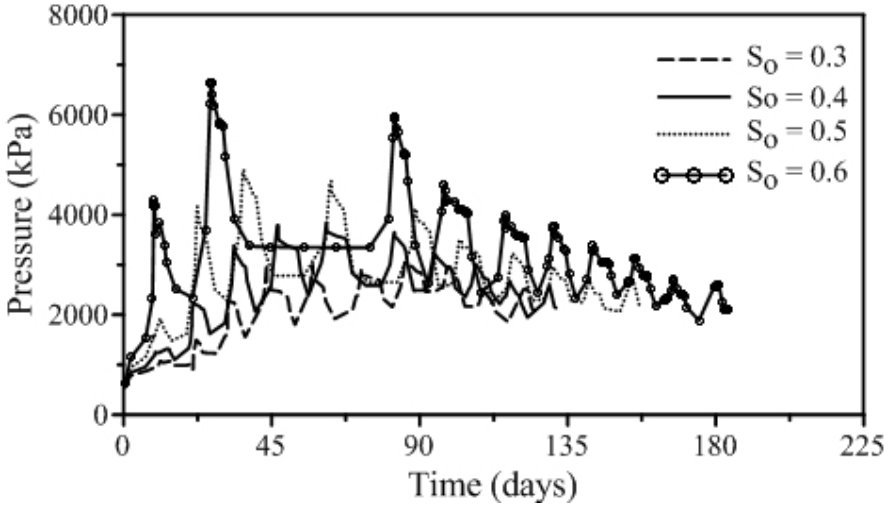

Figure 5. Effect of initial oil saturation on temporal distribution of reservoir pressure.

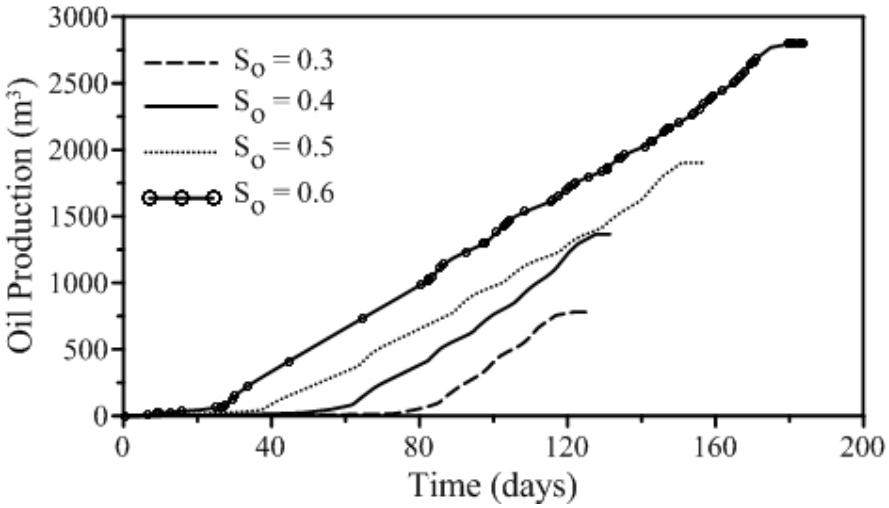

Figure 6. Effect of initial oil saturation on volumetric production of oil.

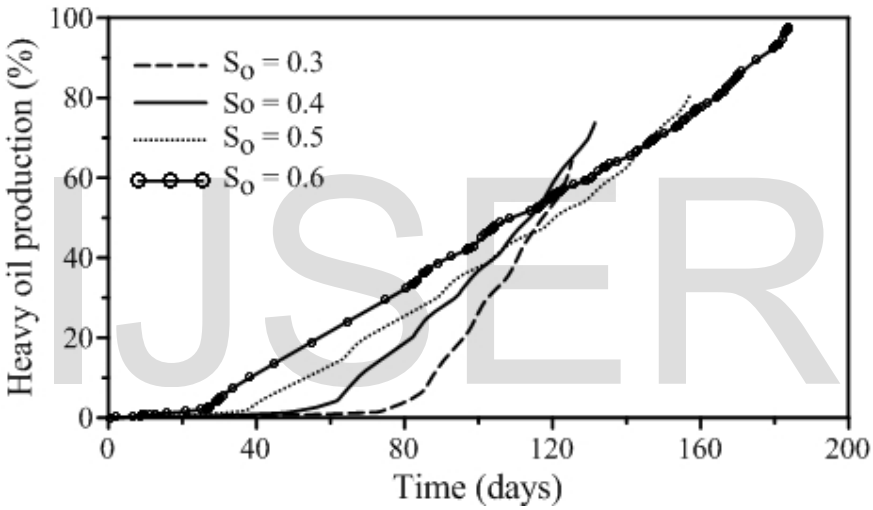

Figure 7. Effect of initial oil saturation on cumulative heavy oil recovery.

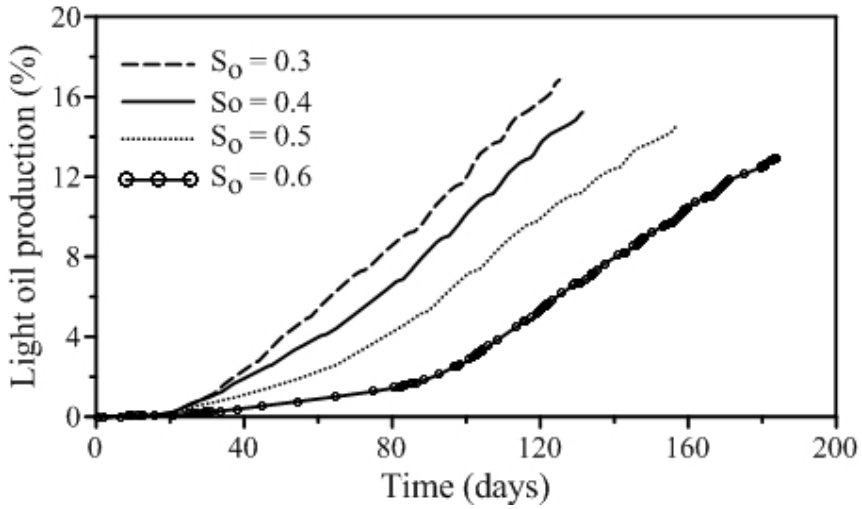

Figure 8. Effect of initial oil saturation on cumulative light oil recovery.